ABSTRACT

Title of Thesis: A UNITED-ATOM REPRESENTATION FOR SPHINGOLIPIDS IN THE CHARMM MOLECULAR DYNAMICS FORCE FIELD

Joshua Lucker, Master of Science, 2023

Thesis Directed By: Professor Jeffery Klauda
Department of Chemical and Biomolecular Engineering

The development of the CHARMM force field (FF) in the late 1970's and early 1980's was groundbreaking at the time. For the first time, a computer program was created that could simulate biological systems on a macromolecular scale. Starting with the simulation of simple proteins, CHARMM has since expanded to include such macromolecules as nucleic acids and lipids, now being able to model complex biological systems and processes. Force fields like CHARMM can be represented in different ways. For example, force fields can be represented through an all-atom representation, in which all atoms in a system are modeled as distinct interaction units. This representation can be simplified into a united-atom representation, which shall be the primary focus of this thesis. A united atom FF has no explicit interaction sites for hydrogen. Instead, the hydrogens are lumped onto the atoms they are connected to, termed 'heavy atoms' as these atoms have a greater atomic weight than hydrogen. The CHARMM FF originally had a united-atom representation for proteins, which was abandoned to focus on all-atom representations. However, in certain cases, such as lipid tails, united-atom representations are often

useful in certain situations; as compared to all-atom representations, united-atom models often speed up simulation times, which is useful in the simulation of large enough systems of molecules. Although there are currently united-atom representations for many types of biomolecules in the CHARMM FF, including multiple types of membrane lipids, there has yet to be a united-atom model for sphingolipids, a type of membrane lipid most commonly found in the myelin sheath of neurons, although its presence has been noted in many types of eukaryotic cells. The goal of this thesis is thus to develop such a model and implement it in the CHARMM FF.

A UNITED-ATOM REPRESENTATION FOR SPHINGOLIPIDS IN THE CHARMM MOLECULAR DYNAMICS FORCE FIELD

by

Joshua Alexander Molloy Lucker

Thesis submitted to the Faculty of the Graduate School of the
University of Maryland, College Park, in partial fulfillment
of the requirements for the degree of
Master of Science
2023

Advisory Committee:
Professor Jeffery Klauda, Chair
Professor Yanxin Liu
Professor Michelle Girvan

Preface

Although a preface is not necessary for most theses, I believe mine would be complete without one. In it, I wish to explain why I am choosing to do a master's thesis in the process of completing a PhD. These past two years have presented many challenges, among them failing to pass my qualifying exam and having to find a different advisor all in the same afternoon. I discussed with the co-director of my program, now my current PhD advisor, whether or not it would be best to finish up with a master's or to continue. After a spring of not knowing where my future was headed, I eventually chose to stay. My now advisor and I then agreed that a master's thesis and defense would still be a good stepping-stone for my academic growth.

I credit four people for inspiring me to continue on. First and foremost, I credit Souad Nejjar, our graduate coordinator, who first encouraged me to continue when I thought I was decided on a master's, and who has encouraged me ever since. Secondly, I credit Prof. Yanxin Liu, whose thoughtful discussions gave me pause to think over what I truly wanted out of my graduate career, and whose research and philosophy inspired me during my time of vulnerability. Thirdly, I credit Prof. Michelle Girvan, whose positive attitude and work ethic has inspired me, and who has been a role model for the type of professor I wish to become. And lastly, but certainly not least, I credit Prof. Jeffery Klauda, who has been gracious enough to take me on as a doctoral student given all my flaws and funding being tight on his end. I am eternally grateful for him giving me a chance to prove my worth, and I know that the completion of my PhD will be because of his guidance and generosity.

Acknowledgements and Dedication

I would first and foremost like to thank and dedicate this thesis to my parents, Drs. Anne Molloy and Jay Lucker, who have helped me overcome many personal battles and who have encouraged me all throughout my life.

Secondly, I would like to thank my committee members, Profs. Michelle Girvan and Yanxin Liu who have graciously agreed to serve on my thesis committee, and who have in their own ways inspired me.

Thirdly, I would like to thank (now) Dr. Yalun Yu who, during the first half of my time that I have been working on this project, has guided and mentored me where needed. I wish him luck in his future endeavors!

Subsequently, I would like to thank Yalun and all others who have provided any data needed in order to complete this project.

I would also like to take this time to thank all of my colleagues, roommates, and otherwise acquaintances who have shown me that it is okay to take a break to hang out with friends once in a while when needed.

Lastly, I would like to thank the two most important people to my success thus far in my graduate school career; Ms. Souad Nejjar for the encouragement and logistical administration needed to complete my master's degree; and Prof. Jeffery Klauda who took me under his wing when I was at my most disheartened, and whose continued guidance has since been an invaluable part of my growth and success as a researcher and graduate student.

I deeply thank each and every one of these people, without whom I would not be here completing and defending my master's thesis.

Table of Contents

Preface ii
Acknowledgements and Dedication iii
Table of Contents iiv
List of Tables v
List of Figures vvi
Chapter 1: Background and Methodology 1
1.1 Background 1
1.1.1 The CHARMM Force Field and Molecular Dynamics 1
1.1.2 Sphingolipids and Sphingomyelins 4
1.1.3 The United-Atom Force Field Model 6
1.2 Methods 8
1.2.1 Dihedral Fitting 9
1.2.2 Bilayer Simulations 12
1.2.3 Bilayer Property Calculations 13
Chapter 2: Results and Discussion 16
2.1 Research Process 16
2.2 Dihedral Fitting Parameters 20
2.3 Bilayer Parameter Results 27
2.3.1 Surface Area per Lipid and Area Compressibility 29
2.3.2 Deuterium Order Parameters (S_{CD}) 31
2.3.3 Electron Density Profiles and Subsequent Properties 34
Chapter 3: Discussion, Conclusions, and Future Directions 38
Discussion and Conclusions 38
Future Directions 39
Bibliography 40

List of Tables

Table 2.1 – Dihedral parameters

Table 2.2 – Surface area per lipid comparison as compared to computational values

Table 2.3 – Surface area per lipid comparison as compared to experimental values

Table 2.4 – Area compressibility comparison

List of Figures

Figure 1.1 – General structure of sphingomyelin

Figure 1.2 – Structure of N-palmitoyl sphingomyelin and N-stearoyl sphingomyelin

Figure 1.3 – Structure of the 'model compounds' used in the dihedral fitting

Figure 2.1 – Surface area per lipid vs. time for SSM at 50 ^{o}C before the dihedral fitting correction.

Figure 2.2 – Probability distributions and PMFs before the dihedral fitting correction.

Figure 2.3 – Dihedral fitting potential energy scans

Figure 2.4 - Probability distributions and PMFs after the dihedral fitting correction.

Figure 2.5 - Surface area per lipid vs. time for PSM at 45 ^{o}C after the dihedral fitting correction.

Figure 2.6 – Comparison of probability distributions for both the model compound and lipid showing that the dihedrals did not fit properly

Figure 2.7 – Deuterium order parameters for PSM

Figure 2.8 – Deuterium order parameters for SSM

Figure 2.9 – Sample Electron Density Profiles for PSM and SSM

Figure 2.10 – Membrane Thickness Comparison

Figure 2.11 – X-ray Scattering Profile for PSM at 45 ^{o}C

Chapter 1: Background and Methodology

1.1 Background

When the original Chemistry at Harvard Macromolecular Mechanics (CHARMM) force field (FF) was released in 1983[1], it revolutionized the field of molecular dynamics. For the first time, a computer program was created that could simulate complex biological systems on the macromolecular level. Since then, CHARMM has been expanded and improved upon, evolving into the force field that we know today[2, 3]. One such expansion of CHARMM that came to be was the formulation of membrane lipids in CHARMM[4-6], along with the subsequent addition of a united-atom force field model for such lipids[7, 8], In the past decade, a united-atom representation for membrane lipids has been introduced, which now includes multiple types of phospholipids[9]. However, other types of lipids, such as sphingolipids, have yet to be included. Thus, in this thesis, we seek to expand upon these models to create a united-atom representation for sphingolipids and sphingomyelins in CHARMM.

1.1.1 The CHARMM Force Field and Molecular Dynamics

Molecular dynamics (MD) originated in the 1950's following the development of the Monte Carlo method at the Los Alamos National Laboratory[10]. Both methods proved useful in the modeling of atomic systems. However, molecular dynamics[11] proved better at simulating the physical processes needed to create complex molecular systems. While Monte Carlo methods often rely on random sampling techniques, (e.g.,

the Metropolis-Hastings algorithm[12]), molecular dynamics uses Newton's equations of motion to simulate the trajectories of atoms, along with the atomic and interatomic potentials, to simulate the forces and potential energies between atoms and molecules.

It was not long before researchers started utilizing molecular dynamics. In 1964, Aneesur Rahman used MD simulations to simulate liquid Argon[13], what is now considered the first realistically simulated MD system[14]. However, it was not until the 1970's when molecular dynamics really started taking off. MD simulations were being applied to many different systems, most notably in the fields of chemical physics and material science[15-18], eventually being used in biophysics to simulate macromolecular biological molecules. In fact, the simulation of the first protein was created in 1977 by Martin Karplus and his colleagues[19]. The subsequent work by Karplus and his research group eventually led to the creation of the CHARMM force field in 1983[1].

CHARMM was among the first force fields to be developed with the idea of biological and macromolecular modeling in mind. In general, force fields are the sets of parameters and equations used in MD (or Monte Carlo methods) to calculate the potential energy of a system of atoms and molecules. Like similar class 1 force fields, such as AMBER[20], GROMOS[21], and OPLS[22], the CHARMM force field takes both bonded and non-bonded potential energies into account. The most recent CHARMM packages have the following potential energy function (equation 1.1), which includes bonds, angles, dihedrals, improper dihedrals, and Urey-Bradley terms for the bonded energies; and van der Waals and electrostatic terms for the non-bonded energies[23, 24]. For reference, the Urey-Bradley term accounts for the 'virtual bond' between the two unconnected atoms of an angle and is used to restrict bond movements in the angle.

$$V = \sum_{bonds} k_b\,(b - b_0)^2 + \sum_{angles} k_\theta\,(\theta - \theta_0)^2 + \sum_{dihedrals} k_\phi\,[1 + \cos(n\phi - \delta)]$$
$$+ \sum_{impropers} k_\omega\,(\omega - \omega_0)^2 + \sum_{Urey-Bradley} k_u\,(u - u_0)^2$$
$$+ \sum_{nonbonded} \epsilon\left[\left(\frac{R_{min_{i,j}}}{r_{ij}}\right)^{12} - \left(\frac{R_{min_{i,j}}}{r_{i,j}}\right)^{6}\right] + \frac{q_i q_j}{\epsilon r_{i,j}} \qquad (1.1)$$

In equation 1.1, the values of k represent the force constants for the bonds, angles, dihedrals, improper angles, and Urey-Bradley terms, and the r-r_0 terms, where r is b, θ, ω, and u, represents how far each of the bonded terms (bonds, angles, impropers, and Urey-Bradley, respectively) are from equilibrium. The non-bonded term involves the Lennard-Jones (van der Waals) and Coulombic (electrostatic) potentials. These terms are not utilized in depth for this project, as the non-bonded forces for lipids have been determined in previous works[6, 8, 9, 25]. For the dihedral term, the n, ϕ, δ terms represent the multiplicity, dihedral angle, and phase shift of the cosine series for each dihedral. We will return to the dihedral term in the methods section.

Since its initial release in 1983, CHARMM has been improved upon and expanded by multiple researchers. The development of CHARMM19[26] in the mid-80's introduced a united-atom model for proteins. This was followed up by the formulation of CHARMM22[23] in the 1990's, which provided a comprehensive all-atom model for proteins. Around the turn of the century, CHARMM27 was released to include nucleic acids and lipids[27]. The development of CHARMM-GUI in the mid- to late-2000's[28, 29] offered a more user friendly interface for researchers to simulate these biological systems (including membranes[30-33]) more easily. The further creation of the

CHARMM General Force Field (CGenFF) a few years later generated the compatibility of CHARMM to be used with drug-like molecules[34].

The development of CHARMM for membrane lipids continued well into the 21st century with the addition and updates of more and more lipids into the most recent CHARMM package (CHARMM36)[5, 6, 25, 35], and eventually included a united-atom compilation of phospholipids (CHARMM36UA[8], and its subsequent recent update, CHARMM36UAr[9]). With all these advancements in CHARMM, there is still room for further expansion. As of now, there is only a united-atom force field for phospholipids in CHARMM among the many types of lipids out there. Therefore, in this thesis, we aim to develop a united-atom model for sphingolipids in CHARMM.

1.1.2 Sphingolipids and Sphingomyelins

Sphingolipids are a type of cell membrane lipid, prominently found in the central nervous system of mammals[36] but have since been found to be crucial components in all types of eukaryotic cells[37-39]. First discovered in brain extracts in the 1870's,[40] sphingolipids have since been found to be key components in the plasma membrane[41, 42]. The most common type of sphingolipid, and the one that will be the primary focus of this research, are sphingomyelins. Sphingomyelins are primarily found in the myelin sheath that surrounds the axons in nerve cells[43]. Sphingomyelins contain three main components: a head group, commonly phosphocholine which contains a phosphate and a charged quaternary methyl ammonium group; a sphingosine backbone, derived from sphingosine, an 18-carbon amino alcohol; and a fatty acid group which contains a carbonyl group and a saturated hydrocarbon chain that varies

between 10 and 20 carbons in length. A visual representation for the structure of sphingomyelin is shown in figure 1.1.

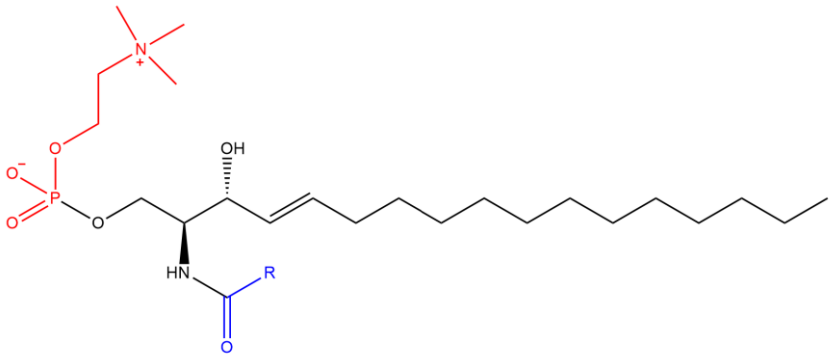

Figure 1.1: The general structure of sphingomyelin. The head group is highlighted in red, the sphingosine backbone is in black, and the fatty acid group is in blue. The R in the fatty acid chain represents a hydrocarbon that is about 10 to 20 carbons in length.

Sphingolipids and sphingomyelins play an important role in the cell membranes of nerve cells [44, 45]. It is thought that sphingomyelin insulates the axons as they carry signals through the neurons[43, 44, 46]. As such, sphingomyelin plays an important role in signal transduction and cell signaling as well[47]. Sphingomyelin is also thought to be present in the inner and outer leaflets of the plasma membrane of all types of mammalian cells and is believed to play important roles in apoptosis and membrane structure in these cells, respectively[48, 49]. Other notable functions of sphingolipids include cell growth[50, 51], stress response[52, 53], and aging[54, 55]. Thus, the simulation of sphingolipids can provide insights into the function and structure of these lipids in human cells, and can be used to research many topical health-related issues.

There are many ways to simulate sphingolipids, and cell membrane lipids in general, using molecular dynamics. One common way sphingolipids are simulated is by modeling all the atoms in the membrane. While this is certainly useful for smaller and mid-sized systems, the larger a system becomes, the longer it takes to simulate, which could be months or even years for some systems. A more practical way to simulate these systems is to simplify the lipids. For example, one common method that is used is coarse-grained modelling. A common coarse-grained force field used in this case is MARTINI[56]. In such coarse-grained force fields, portions of the lipids (usually a sizable group of atoms) are lumped together as one interaction site. While this certainly cuts down on simulation time and is useful for larger membrane simulations, some accuracy is lost in coarse-grained simulations. If one wishes to keep their simulations as accurate as possible while keeping simulation times reasonable, the united-atom model, described below, can be a useful alternative.

1.1.3 The United-Atom Force Field Model

A united-atom simulation model is a type of force field representation in molecular dynamics in which the hydrogen atoms on a molecule are lumped onto the 'heavy atom' (non-hydrogen atom) that they are connected to. It is one of three main types of force field representations used in molecular dynamics, along with all-atom and coarse-grained force field modeling. An all-atom representation involves modeling all the atoms in a molecular system as distinct interaction sites, whereas a coarse-grained representation involves distinct groups of atoms being lumped into one unit for computational simplicity and simulating ease. In fact, united-atom force field modeling

is often thought of as the simplest type of coarse-graining, which can range from hydrogens to entire molecules being lumped as one unit. More information about the differences between these modelling types, specifically for lipids, can be found here[57].

There are advantages and disadvantages to each type of force field representation. An all-atom representation is the most accurate but can take an excessive amount of time to simulate. Thus, it is often useful to simplify the molecules in the system to speed up simulations, especially for larger systems. An extensive coarse-graining can be helpful but often leads to less than ideal accuracies in the system, especially if the system is small or mid-sized. In small or mid-sized cases, a united-atom system is usually the most practical to use. In general, a united-atom simulation shortens the computational time, in many cases by as much as half the time of an all-atom simulation of comparable size, without much loss to accuracy.

United-atom force field models have also been utilized in such force field families as GROMOS, OPLS, and CHARMM to simulate membrane lipids[58, 59, 6]. However, in each of these FF families, phospholipids were the primary lipids that were included. While there are united-atom models for sphingolipids that exist, most notably in GROMOS[60, 61] (which is solely a united-atom force field package), the representation of sphingolipids as united-atom is highly underutilized. We thus aim to implement such a representation in CHARMM, adding to the CHARMM36UAr force field where a united-atom model for phospholipids has recently been implemented[9].

1.2 Methods

As mentioned, the purpose of this thesis is to create a united-atom representation for sphingolipids in the CHARMM force field. To do this, the two tail groups (sphingosine backbone and fatty acid group) of two common sphingomyelins, N-palmitoyl sphingomyelin (PSM) and N-stearoyl sphingomyelin (SSM) were taken from the CHARMM36 all-atom force field package and converted to a united-atom framework. We shall then see that this conversion can easily be adapted to the other sphingolipids in CHARMM to create a complete united-atom sphingolipid force field. The head (phosphocholine) group was not converted to united-atom due to its complexity and the nature of the polarity and charges that would been lost if converted. The difference between the structure of PSM and SSM is the length of their fatty acid group; PSM has a 16 carbon fatty acid chain whereas SSM has an 18 carbon fatty acid chain. Figure 1.2 shows the structure of PSM and SSM, with the specific portions that were converted to united-atom highlighted in red.

To convert to a united-atom framework, the hydrogens for the specified atoms were removed and the heavy atoms they were connected to (in this case, carbons) were replaced with a united-atom carbon-hydrogen combined unit. The notation CH#E was used for these units as is consistent with previous CHARMM united-atom packages, where # was replaced with the number of hydrogens in the carbon-hydrogen unit. The parameters of each unit, as listed in equation 1.1, were then determined. Wherever possible, the parameters for the bonded and nonbonded forces were taken from the previously defined CHARMM36 and CHARMM36UAr force field packages for the all-atom and united-atom portions of the lipid, respectively. However, at the all-atom

and united-atom interface, although the bonds, angles, and non-bonded forces could be conserved, the dihedrals were not provided and had to be determined through a dihedral fit, as will be described later. After the conversion, the new united-atom sphingolipid framework was compared against the established all-atom framework.

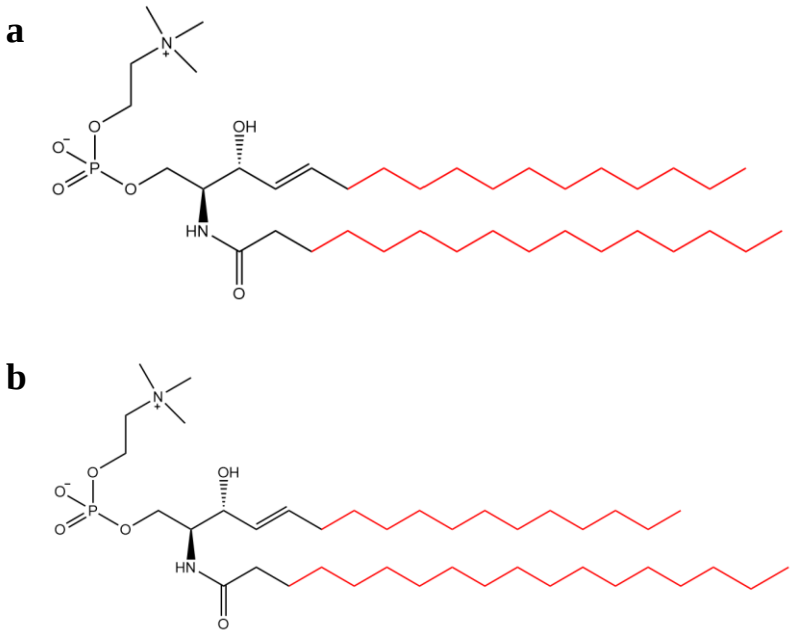

Figure 1.2: The structure of N-palmitoyl sphingomyelin (PSM, top) and N-stearoyl sphingomyelin (SSM, bottom). The united atom portions are labeled in red.

1.2.1 Dihedral Fitting

As mentioned previously, most of the parameters for the new sphingolipid force field model could be taken from the CHARMM36 and CHARMM36UAr packages. However, most of the dihedral parameters at the united-atom and all-atom interface had not been previously defined and as such needed to be found using a dihedral fit. A dihedral fit, along with including accurate formulations for the dihedral angles, also provides an energy correction that would be lost otherwise and lead to inaccurate

results. Essentially, we need to fit the dihedral parameters k_ϕ, n, and δ in the dihedral term of equation 1.1. To perform a dihedral fit, the potential energy scan of a specific dihedral is fit to a target scan, usually that of the quantum mechanical potential energy scan. However, keeping consistent with the CHARMM36UAr model,[9] the target potential energy scans in this case were those of the corresponding all-atom dihedrals.

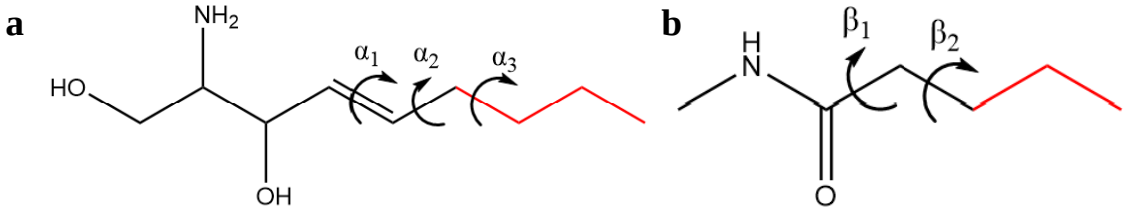

Figure 1.3: Model compounds for the dihedral fit of the sphingosine chain (left) and fatty acid chain (right). The united-atom portions are labeled in red.

To start, two small 'model compounds,' one for each tail group, were created that included each of the dihedrals of study. These compounds along with corresponding labeled dihedrals are shown in figure 1.3. When creating the compounds, the regional structure and properties around the dihedrals were kept the same as those corresponding to the sphingomyelins so that an accurate all-atom target energy scan could be created. The atoms on each model compound that corresponded to a united-atom unit in the sphingomyelins were then converted and a potential energy scan was taken for the updated models. As is typical in a potential energy scan, both a forward and backward scan (from 0^o to 360^o and from 360^o to 0^o) was taken, and the minimum energy from each scan was used to construct an overall potential energy scan. During these scans, the dihedrals not being scanned were left unconstrained to allow

for free movement of these dihedrals. A dihedral fit was then conducted using a code from Professor Alexander MacKerell's group at the University of Maryland, Baltimore that uses a simulated annealing method[62]. For each compound, the dihedrals were fit iteratively until the parameters ceased to change. Afterwards, these new parameters were implemented into the new united-atom model, and the simulations for this model were run and compared to those of the CHARMM36 all-atom model.

To assure that the dihedral parameters were accurate, probability distributions and potentials of the mean force (PMFs) were calculated for both the all-atom and united-atom model compound simulations. The probability distributions displayed the likelihood that a specific dihedral had a specific angle value between -180^o and 180^o in each simulation. The PMFs, which determined the amount of energy at each angle value, could then be calculated from the probability distributions at each angle using the equation $-k_BTln(P)$. In this equation, k_B is Boltzmann's constant, T is the temperature of the simulations, and P is the probability from the probability distribution. Ideally, the shape of the PMFs should be the same as those of the dihedral energy scans, and the PMFs for the united-atom model compounds should match those of the all-atom model compounds. The probability distributions were originally calculated using the FFLiP program developed by Yalun Yu, a recent graduate of our lab[63]. However, when the University of Maryland switched over to Zaratan in September of 2022, there were compatibility issues with the new supercomputer and FFLiP. Thus, a new PMF/probability distribution code was coded and used in its place.

1.2.2 Bilayer Simulations

In this work, two common sphingomyelins, PSM and SSM, were simulated via both all-atom and united-atom force field depictions. PSM models were simulated at 45, 48, and 55 ^{o}C, and SSM models were simulated at 45, 50, 55, and 65 ^{o}C, with three simulations being run for each of the seven temperatures. The temperatures were specifically chosen to compare with recent experimental and computational literature related to sphingolipids[25, 64]. Each simulation included 80 lipids, 40 for each membrane layer, and between 2400 and 2800 water molecules. Keeping consistent with the CHARMM family, the modified TIP3P water model was used to simulate water[65, 66]. These lipid bilayer simulations were conducted in NAMD[29, 67] for the use of parallel computing on supercomputers. All simulations were run on the University of Maryland's supercomputers, Deepthought 2 and its successor Zaratan, and on Rockfish, a supercomputer at Johns Hopkins University. Each simulation was initially run for 250 ns and extended as needed until at least 100 to 150 ns of equilibrated data was generated. The equilibrated data was then used to calculate certain bilayer properties, as described in section 1.2.3.

In general, the properties of the simulations were kept the same as that of CHARMM36UAr[9]. A force-based switching function was used to change the van der Waals forces to zero between 10 and 12 Å, whereas electrostatics over 12 Å utilized the particle mesh Ewald (PME) method[68]. In simple terms, PME is a computational physics method that uses the Fourier Transform to algorithmically calculate long-range interactions. The simulations utilized an NPT ensemble (number of molecules, pressure, and temperature all kept constant), where pressure (P) was 1 bar. For *XY*

lengths in the simulation, the two sides were set equal to each other, which were both allowed to change independently of the *Z*, yielding a semi-isotropic simulation cell. In NAMD, Langevin dynamics, which uses stochastic differential equations to model systems of molecules, was used to maintain constant temperature via the Nosé-Hoover thermostat method[69], and the Nosé-Hoover Langevin piston algorithm, a variation of the Nosé-Hoover thermostat for pressure fluctuation control, was used to maintain constant pressure.[70, 71]

The initial all-atom simulations were created using CHARMM-GUI[28] and equilibrated and run with NAMD. United-atom topology and parameter files were then adapted from previous all-atom and united-atom topology and parameter files. Using these files, a sample frame from the equilibrated all-atom simulations could then be converted to a united-atom framework, and united-atom simulations could be run using NAMD in a similar method to the all-atom simulations. From these simulations, certain bilayer properties, such as surface area, area compressibility, hydrogen bonding, and other properties could be calculated for both the all-atom and united-atom simulations. These properties are discussed in depth in the next section.

1.2.3 Bilayer Property Calculations

In order to test the accuracy of the new united-atom sphingolipid model, some common bilayer properties were determined from both the all-atom and united-atom simulations described previously and were then compared to recent experimental and computational values. Two bilayer properties that were determined were the surface area per lipid (SA/lip) and area compressibility (K_A). The surface area per lipid was

calculated as the area of a simulation cell along the x and y plane divided by the number of lipids per leaflet. The area compressibility was then calculated using equation 1.2, where k_B is the Boltzmann constant, T is the temperature, <A> is the average of the total area, and $<\delta A^2>$ is the mean square deviation of this area. The surface area per lipid gives insights to the intermolecular forces in the membrane, whereas the area compressibility gives insights into the elasticity of the membrane.

$$K_A = \frac{k_B T \langle A \rangle}{\langle \delta A^2 \rangle} \tag{1.2}$$

Another bilayer property that was studied was the hydrogen order parameters (S_{CH}). This value is calculated from equation 1.3, where brackets represent the ensemble and time averages, and θ represents the angle between the carbon-hydrogen, or carbon-deuterium bond, and the bilayer normal plane. In the united-atom, these hydrogens were restored according to their ideal geometries, as was done in the original CHARMM36UAr[9]. Comparing order parameters to experiments can give insight into the accuracy of the molecular dynamics simulations.

$$S_{CH} = \left| \langle \frac{3}{2} \cos^2 \theta - \frac{1}{2} \rangle \right| \tag{1.3}$$

The final set of properties that were utilized in this thesis were the Electron Density Profiles (EDPs) and subsequent properties. The EDPs portray the distribution of the different lipid functional groups and water molecules through the membrane for each simulation. From the EDP, the membrane thickness can be calculated three different ways: the distance between lipid headgroups (D_{HH}) measured by the distance between the overall membrane peaks in the EDP, the overall bilayer thickness (D_B) calculated as the distance between the water EDP midpoints, and twice the hydrophobic

thickness ($2D_C$) where D_C is estimated as halfway between the midpoints of the tail groups. From the EDPs, the X-ray scattering form factors can also be calculated using a Fourier transform of the EDPs, calculated using the SIMtoEXP program[72]. The membrane thicknesses and form factors can then be compared to experimental data[64].

The following chapter provides the results and findings from these simulations and corresponding bilayer parameters, along with the results from the dihedral fitting and some of the problem solving that came about during the collection of these results. We then discuss these results along with the expected outcomes and future directions for this project in the final chapter of the thesis.

Chapter 2: Results and Discussion

2.1 Research Process

During the development of this thesis, there were multiple obstacles that had to be overcome. The purpose of this section is thus to describe the process of conducting the research for this thesis as well as the problem-solving methods conducted to overcome these hurdles. To start out the research, all-atom simulations of PSM and SSM were set up and run in order to compare to that of the literature as well as to have current data with which to compare the united-atom simulations. After running these simulations, the next step was to conduct the dihedral fitting for the united-atom simulations. As it would turn out, the dihedral fitting ended up being the limiting step, as many challenges arose in the process of conducting the fits.

After running the initial dihedral fitting and dihedral parameters found, united-atom simulations were run. However, the simulations resulted in an equilibrated surface area per lipid reading well below 50 $Å^2$ for all simulations. For reference, the surface areas per lipid for the all-atom simulations are around 55 $Å^2$ and experimentally is around 60 $Å^2$. A surface area per lipid below 50 $Å^2$ usually indicates that the lipid is transitioning into the gel state, which should happen at around 40^{o}C, not 50^{o}C. It should be noted here that the all-atom simulations were developed before sufficient experimental surface areas per lipid were studied. As such, the all-atom simulations are based on prior chain order parameters, which have since been updated along with the experimental surface areas per lipid in a recent paper by Doktorova et. al.[64]. I will discuss this later in the thesis, and it is noted that the all-atom force field for

sphingolipids needs to be modified, with plans to do so in the near future. A plot of surface area per lipid vs time for a trial of SSM at 50°C is shown in figure 2.1 (left).

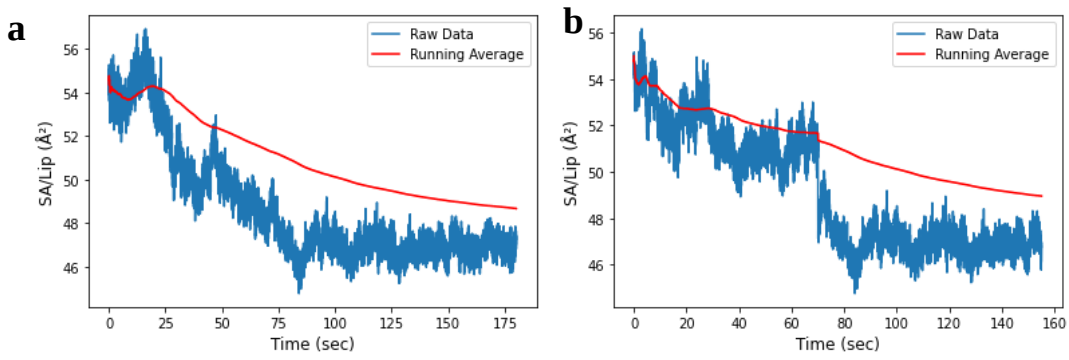

Figure 2.1: Two plots of SA/lip vs time for a sample trial of SSM at 50 °C, showing a gradual decrease to around 46-48 $Å^2$ as the system equilibrated. The left shows the plot when the double bond in the sphingosine chain was part of the united-atom portion of the lipid, and the right shows the plot when the double bond was changed to all-atom. No significant difference is found between the two.

From here, the potential root of this problem was investigated. It was initially examined whether the root of the problem was due to where the united-atom cutoff was determined. At the beginning of the project, it was debated where the cutoff between the united-atom and all-atom portions of the lipid tails should be. For the fatty acid chain, the united atom cutoff was decided to be right below the carbon adjacent to the carbonyl group, as this carbon in particular is still affected by the polarity of the carbonyl group, and as this was the cutoff determined in previous fatty acid chains in CHARMM36UAr. It was debated where the cutoff for the sphingosine chain should be, as a cutoff right above the double bond cuts very close to the polarity in the upper

portions of the sphingosine chain. However, it would be ideal for as much of the sphingosine chain to be converted to a united-atom representation as possible. As such, simulations were run for both representations to see whether the dihedral fit issue could be resolved by choosing the representation that produced a better fit. However, neither representation produced a dihedral fit that was ideal, as shown in figure 2.2 for PSM at 45 ^{o}C.

It was at this point when it became apparent that the problem was most likely due to something more fundamental occurring with the dihedral fit itself. FFLiP, a force field optimization package developed by a recent graduate of the Klauda Lab, Yalun Yu, was originally used to assess the goodness of fit. In this package, the probability distributions of the dihedral angles could be calculated and evaluated as well as the PMFs, as described in section 1.2.1. Ideally, the probability distribution and PMFs for both the all-atom simulations and united-atom simulations should match. However, as shown in figure 2.2, the distributions and PMFs did not match for the dihedrals of the sphingosine chain. The double bond for the all-atom double bond simulations showed slight variations about d2 (the double bond) when it should be rigid at 180^{o}, and both the united atom and all atom double bond cutoffs showed no peak for d3 at around 0^{o} where the completely all-atom simulations show a significant peak. To fix this problem, the model compound for this chain needed to be studied. The all-atom double bond representation was chosen to continue due to the proximity of the united-atom cutoff in the united-atom double bond representation to the polarity of the hydroxyl group.

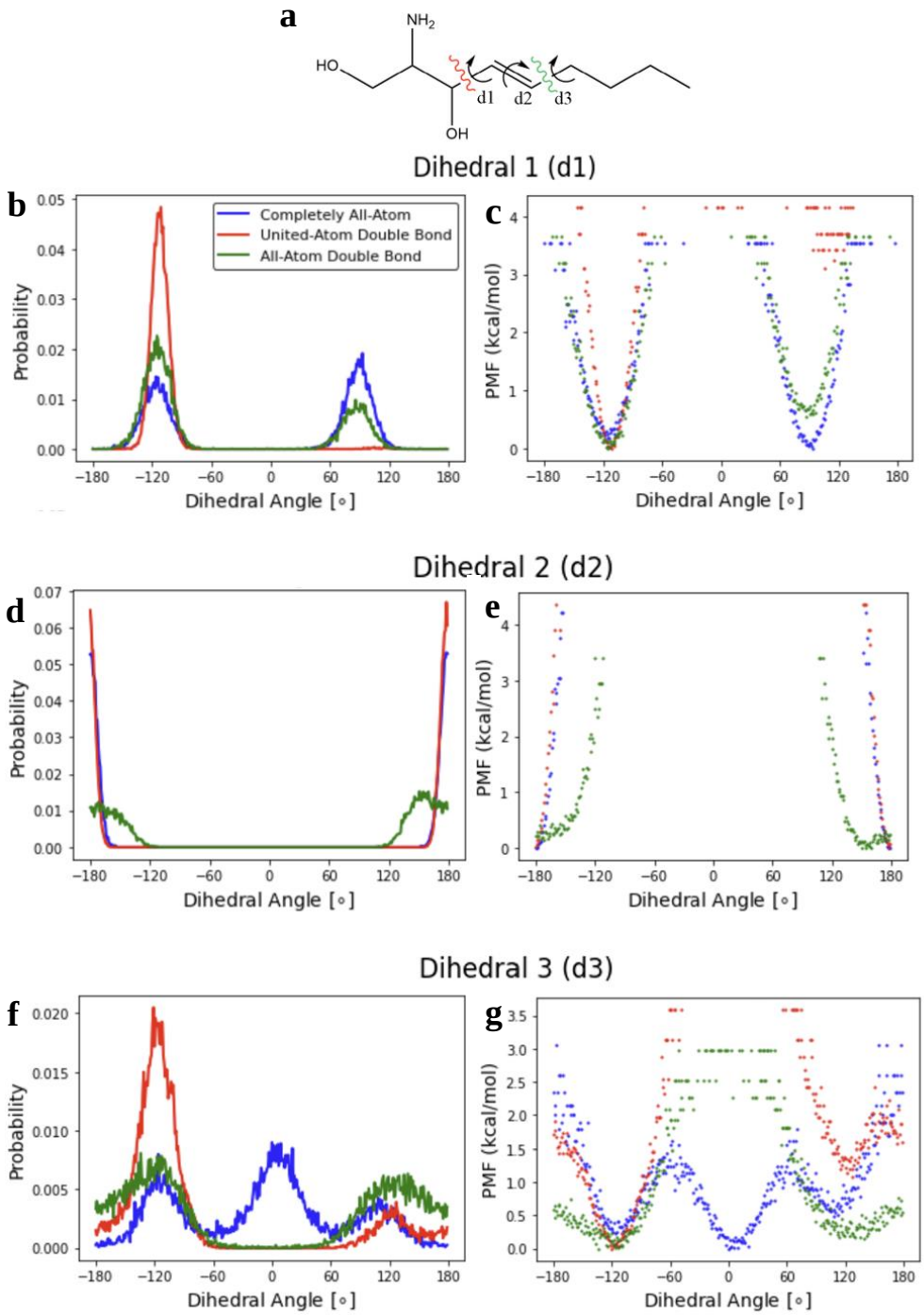

Figure 2.2: Probability distributions (left) and PMFs (right) of the completely all-atom simulations, united-atom simulations with a cutoff right above (or to the left in the top diagram) the double bond, and united-atom simulations with the cutoff right below (to the right in the top diagram) the double bond for PSM at 45 ºC

Model compound simulations were initially constructed using CHARMM-GUI's[28] Multicomponent Assembler. However, these simulations produced constant probability distributions and inaccurate results for the united-atom simulations. Initially thinking that this was an issue with the FFLiP program, it was decided to take a deeper look at this program. After a deeper look, it was found that there were possible compatibility issues with CHARMM-GUI and the united-atom model compounds, and thus, the model compounds were instead simulated manually.

Around this time, the University of Maryland released its new supercomputer, Zaratan, where there ended up being compatibility issues with the FFLiP program and the updated software on the supercomputer and a new code for the probability distribution and PMF was created. While writing the code, it was postulated that perhaps the root of the problem was that the dihedrals had not been properly zeroed in the dihedral fitting. When doing a dihedral fit iteratively, it is commonplace to zero out the dihedral of study as to not introduce any multiplicities or other additional values. As the dihedrals seemed to be fitting properly, it was not thought that this would be a problem. With this problem now fixed, better dihedral fitting results were found, as discussed in section 2.2 below.

2.2 Dihedral Fitting Results

As mentioned in section 1.2, when converting the topology and parameters for PSM and SSM, most of the parameters and topologies had been previously established in CHARMM36 and CHARMM36UAr files, and thus each of these parameters could be easily adapted for use in the all-atom and united-atom portions of the molecules,

respectively. At the interface of the all-atom and united-atom portions of the lipids, the bonds and angles had been previously established in the original formulation of the CHARMM36UAr force field or could be easily adapted from the CHARMM36 all-atom force field. However, for most of the dihedrals at this interface, the parameters had not been previously established. These dihedral parameters needed to be optimized due to the nature of the cosine series of the dihedrals, as shown in equation 1.1. As mentioned in section 1.2.1, this optimization also induced an energy correction that would otherwise make the united-atom model inaccurate, as we see in section 2.1. Thus, the dihedral parameters could not be transferred from previous models as the bonds and angles were and had to be determined using a dihedral fit.

The method of a dihedral fitting is discussed in depth in section 1.2.1. In short, the dihedrals were separated into two model compounds, one for the sphingosine chain and one for the fatty acid chain as shown in figure 1.3, using similar properties and corresponding all-atom/united-atom portions of the compounds. A potential energy scan was then formulated for each dihedral, and these scans, or potential energy surfaces, were fit as best as possible to those of their corresponding all-atom dihedral surfaces iteratively using a simulated annealing method, from which we could get the dihedral parameters. In all, there were six dihedrals that crossed the all-atom and united atom interface. The specific dihedrals that were studied are shown in figure 1.3. One dihedral (adjacently to the right of β_2 of the fatty acid chain) was not studied as it was previously found in the CHARMM36UAr force field. The dihedral fits for the potential energy curve of the other five dihedrals are shown in figure 2.3.

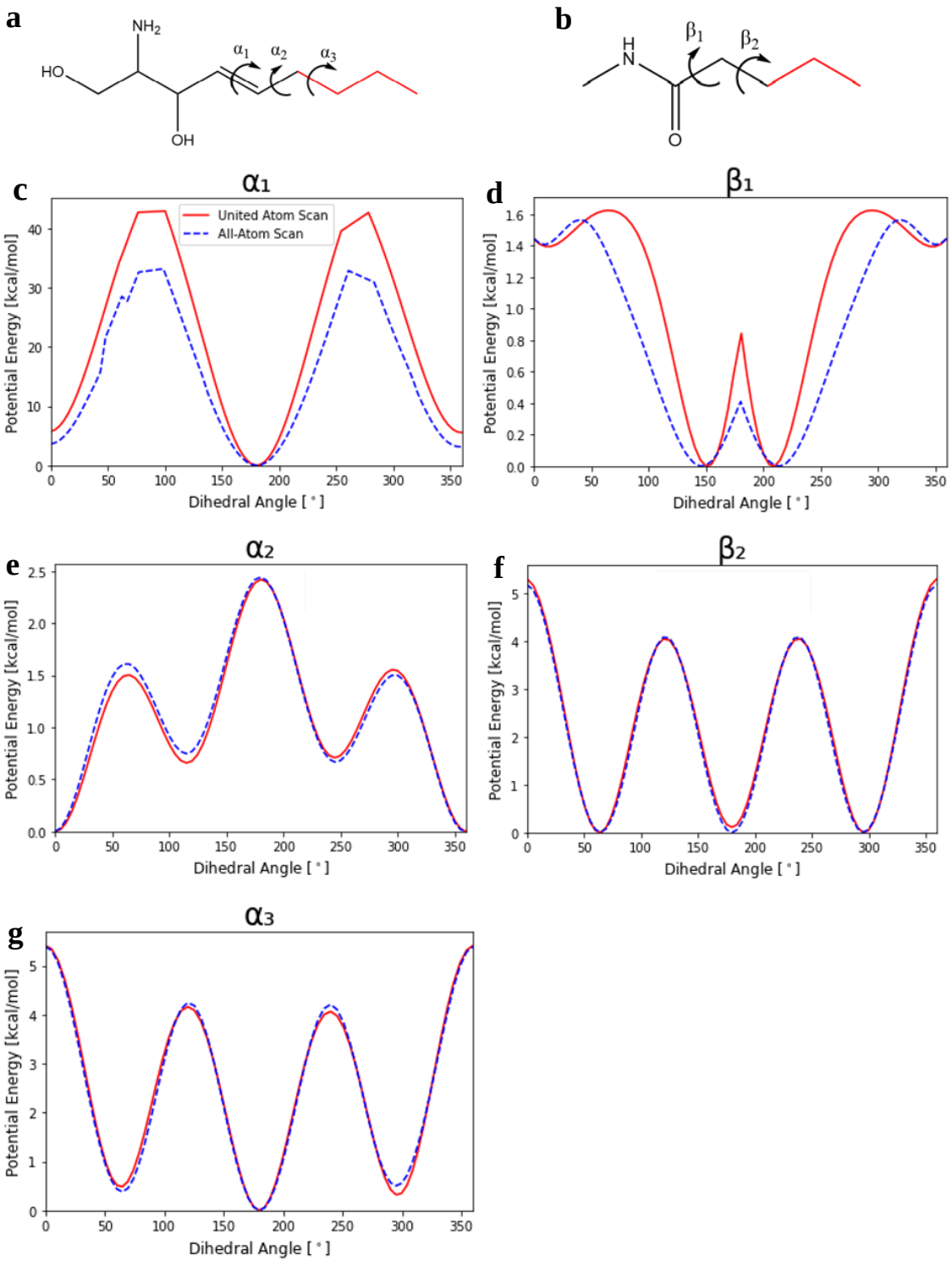

Figure 2.3: Dihedral Potential Energy Scans for the dihedrals of the sphingosine chain (left) and fatty acid chain (right), corresponding to those in figure 1.3.

As a recap, recall the portion of the CHARMM potential energy equation that lists the energy of the dihedral angles (equation 2.1). It should be noted that each dihedral can have multiple multiplicities, as shown in table 2.1, all of which were kept the same as their all-atom counterparts. Note also that a δ of 180 shifts the cosine 180 degrees, essentially negating the cosine and making the dihedral term negative.

$$\sum_{dihedrals} k_\phi \left[1 + \cos(n\phi - \delta)\right] \qquad (2.1)$$

Overall, we find that each set of dihedral parameters produces a good fit to the all-atom scan (figure 2.3). For the β_1 angle, the potential energy scan has higher peaks at approximately 90° and 270° for its united-atom counterpart, along with narrower wells at about 145° and 215°. This is believed to be due to some of the missing dispersion force charges that resulted from the lumping of the hydrogens onto the carbon atoms in the united-atom portion of the lipid. It is thought that the hydrogens that were removed near the all-atom/united-atom interface, which had a small positive charge, interacted with the oxygen and nitrogen in the amide group of the fatty acid chain, stabilizing these regions in the all-atom representation. This produces a less than ideal fit, but one that is still produces practical results. Table 2.1 shows the dihedral parameters resulting from this fit. We also find that for the dihedral going over the double bond (α_1), the united-atom energy scan is much higher than that of the all-atom energy scan. However, the key portion of fitting this angle is that the well at 180° is high and narrow to produce a rigid double bond. In fact, we find this fit better compared to a more overlaying fit, as the latter produces a less ideal, more flexible double bond as seen in dihedral 2 in figure 2.2. The former produces ideal PMFs and probability distributions for this angle, as we shall see in figure 2.4.

Table 2.1: Dihedral Parameters for Each Fitted Dihedral

	α_1		α_2			α_3			β_1			B_2		
n	1	2	1	2	3	1	2	3	1	2	3	1	2	3
k_ϕ	1.11	12.99	1.90	0.75	0.58	1.50	0.47	2.03	1.00	1.94	0.16	2.13	0.62	1.28
δ	0	180	180	180	180	180	180	0	0	180	180	180	180	0

As mentioned, to assess the goodness of fit, the PMFs and probability distributions were calculated again for these new parameters for the sphingosine model compound to compare to those of the 'problem' dihedrals as shown in figure 2.2. These PMFs and probability distributions are provided in figure 2.4. As compared to figure 2.2, we find better fits for the dihedrals in the sphingosine chain of the model. The double bond is rigid for the model compound, and the missing peak for the third dihedral at 0^o is not missing. The PMF and probability distribution plots for the all-atom/united-atom hybrid of this compound almost completely overlap with those of the completely all-atom simulations. As such, the model compounds now are completed and all that is left is for them to be scaled up for full lipid simulations.

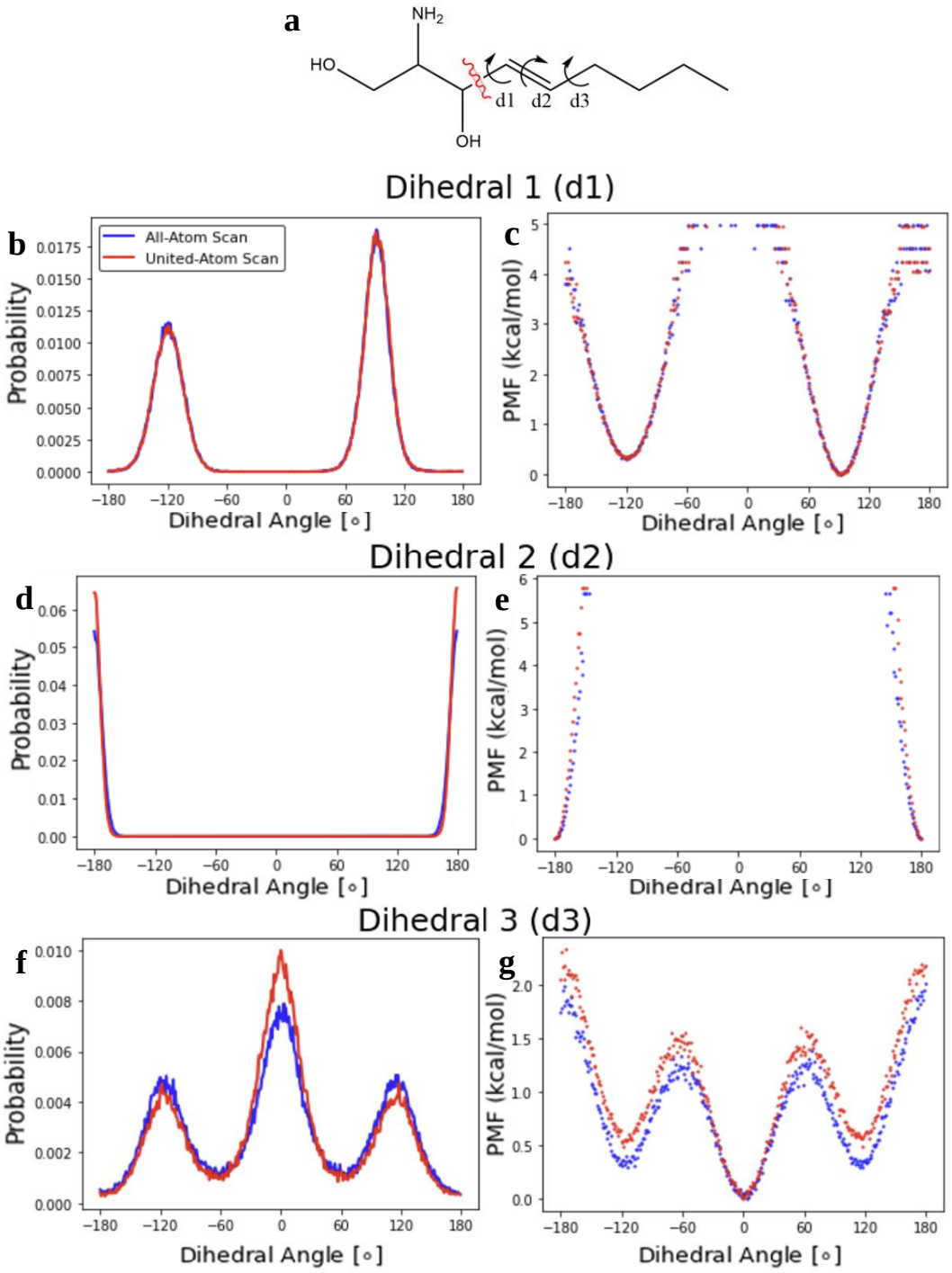

Figure 2.4: Probability distributions (left) and PMFs (right) for the 'problem' dihedrals of the sphingosine model compound. As one can see, the updated scans for these dihedrals match up significantly better as compared to those in figure 2.2.

After fitting the dihedrals for the all-atom double bond simulations, a sample simulation for PSM at 45°C was then run, where the surface area per lipid had indeed improved, now showing an overall value of around 55 $Å^2$ (see figure 2.5 below) similar to that of the all-atom simulations. Now with the dihedral parameters found and the parameters and topologies provided, the PSM and SSM simulations could then be converted to a united-atom representation and run, as described in section 1.2.2. The bilayer parameter results of the united-atom simulations could then be calculated and compared with the all-atom simulations, as shown in section 2.3.

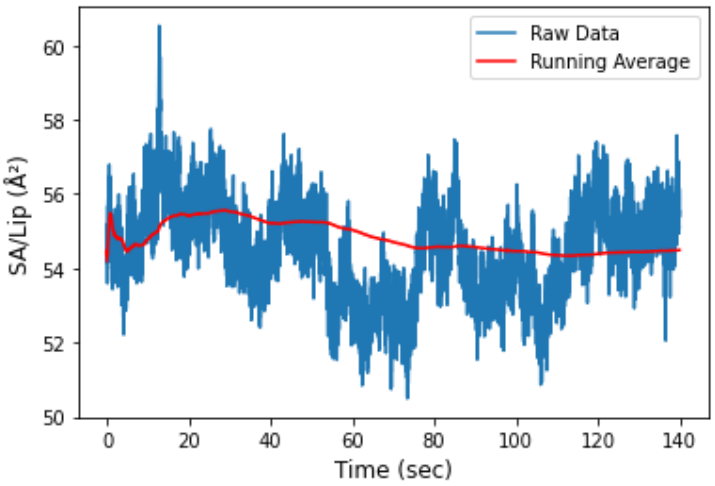

Figure 2.5: Plots of SA/lip vs time for a sample trial of PSM at 45 °C. Note for this plot that, compared to the plots in figure 2.1, the surface area per lipid stays mostly constant around 55 $Å^2$. The surface area per lipid is allowed to change slightly as the system equilibrates and evolves over time.

2.3 Bilayer Parameter Results Thus Far

Below are the results of the bilayer lipid parameters, as described in section 1.2.3. As mentioned in section 1.2.2, PSM simulations were run at 45, 48, and 55 ^{o}C, and SSM simulations were calculated at 45, 50, 55, and 65 ^{o}C. Three trials were run for each temperature, and parameters were calculated from these trials and compared to recent computational and experimental values[25, 64]. The parameters that were included in this paper were the surface area per lipid (SA/Lip), area compressibility (K_a), deuterium order parameters (S_{CD}), Electron Density Profiles (EDP), X-ray Scattering Profiles, and membrane thickness. It should be noted that the lipid bilayer simulations are in progress, as the dihedrals for the sphingosine chain of the lipid bilayer simulations did not carry over properly (figure 2.6). It is uncertain whether this is a discrepancy in the lipid itself or a result of the bilayer. Simulations are currently running to see whether this is a result of the lipid itself or the bilayer. However, we provide what we have so far for each parameter in the sections below.

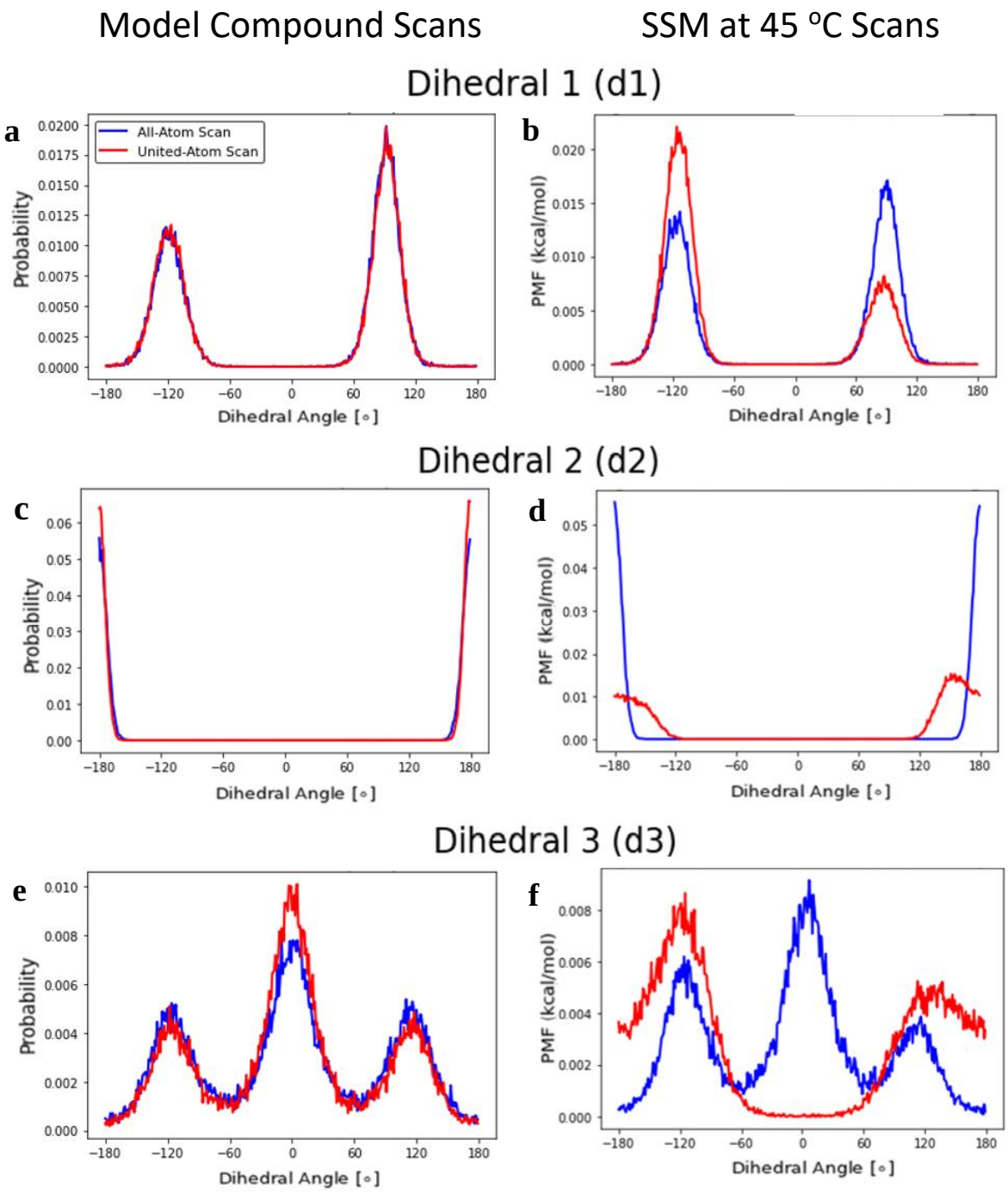

Figure 2.6: When transferring over the dihedral parameters from the model compounds to the lipid bilayer simulations, it was found that there was some discrepancy in the lipids that did not allow the dihedrals to fit properly. This discrepancy is shown here in a comparison of the probability distributions.

2.3.1 Surface Area per Lipid and Area Compressibility

The SA/Lip values for both the all-atom and united-atom simulations are provided in tables 2.2 and 2.3 below. Table 2.2 shows the comparison of the parameters at the corresponding temperatures to that of previous all-atom computational values in CHARMM36 for sphingolipids[25], and table 2.3 shows the parameters at the corresponding temperatures to that of recent experimental values by Doktorova et. al.[64] In table 2.2, one can see that our current all-atom values match quite nicely with those of recent computational values. The values for the united atom simulations for SSM at 50 ^{o}C also matches quite nicely to current and recent computational all-atom values. However, for the united-atom simulations for both SSM at 45 ^{o}C and PSM at 48 ^{o}C, the surface area per lipid is much lower than that of its all-atom counterparts. This is most likely due to the phase transition from the liquid to the gel phase, which should happen around 40 ^{o}C, but is happening around 50 ^{o}C due to the dihedrals not fitting properly for the lipid simulations. In table 2.3, we find again that temperatures below 50^{o}C transitioned into the gel phase for the united-atom simulations. However, those above 50^{o}C showed comparable surface areas per lipid to that of the recent computational all-atom simulations, and in many cases, higher surface areas per lipid, climbing up toward those of the recent experimental values. It should be noted that the all-atom representation for sphingolipids was formulated before the release of the recent experimental data, which is why the surface area per lipid is lower than expected. As such, as force field adjustment is warranted for this representation as well.

For area compressibility, experimental values were not provided, but recent computational values are given. For these values, we find that the all-atom simulations

are quite comparable with that of the recent computational data for sphingolipids. For the united-atom simulations, we find the area compressibility quite high for those simulations below 50 ºC, which is due to the simulations being in the gel phase at these temperatures, which overall leads to higher compressibility. The area compressibility for SSM at 50ºC is lower than that of the all-atom simulations. This is consistent with the CHARMM36UAr model being utilized, which finds overall lower compressibilities in the model[9].

Table 2.2: Surface Area per Lipid Values Compared to Previous CHARMM Values

SA/Lip (Å^2)	All-Atom Simulations	United-Atom Simulations	Previous CHARMM[25]
PSM @ 48 ºC	55.4 ± 0.4	49.2 ± 0.0	55.4 ± 0.2
SSM @ 45 ºC	52.8 ± 0.5	48.2 ± 0.3	54.5 ± 0.2
SSM @ 50 ºC	55.6 ± 0.2	55.1 ± 0.1	55.4 ± 0.2

Table 2.3: Surface Area per Lipid Values Compared to Recent Experimental Values

SA/Lip (Å^2)	All-Atom Simulations	United-Atom Simulations	Recent Experiments[64]
PSM @ 45ºC	54.9 ± 0.2	50.6 ± 0.6	60.0 ± 2%
PSM @ 55ºC	56.5 ± 0.2	56.4 ± 0.2	61.9 ± 2%
SSM @ 55ºC	56.2 ± 0.2	57.4 ± 0.21	62.5 ± 2%
SSM @ 65ºC	57.9 ± 0.1	58.8 ± 0.1	64.9 ± 2%

Table 2.4: Area Compressibility Values for All-Atom and United-Atom Simulations

Area Compressibility (N/m)	All-Atom Simulations	United-Atom Simulations	Recent Experiments[64] (where provided)
PSM @ 48°C	0.60 ± 0.05	1.86 ± 0.00	0.35 ± 0.05
SSM @ 45°C	0.62 ± 0.15	1.15 ± 0.39	0.29 ± 0.04
SSM @ 50°C	0.44 ± 0.04	0.26 ± 0.01	0.44 ± 0.06

2.3.2 Hydrogen Order Parameters (S_{CH})

Order parameters are presented below in figure 2.7 for all experimental and computational comparisons that were provided. The experimental comparisons come from a recent paper by Doktorova et. al.[64], whereas the computational comparisons come from the original CHARMM36 paper for all-atom sphingolipids[25]. Order parameters are given for PSM at 45, 48, and 55 °C, and SSM at 45 and 50 °C. Experimental data was given only for PSM, whereas computational data was given for SSM. For the experimental literature (PSM), only the fatty acid chain was provided for comparison. For each temperature, the all-atom, united-atom, and experimental and computational data are shown on the same graph for comparison.

As one can see, the recent all-atom simulations conducted in this research match up almost exactly with previous all-atom computation, which is to be expected as both simulations were conducted using very similar metrics. For the united-atom simulations, it should be noted that a lower surface area per lipid also produces higher chain order parameters. This is why many of the lower-temperature united-atom simulations which show lower surface areas per lipid also show higher order

parameters. There is thus a need to further examine and fix the dihedrals for the lipid simulations, which will be examined in the near future. For the higher temperatures, we find that the united-atom simulations show lower order parameters, suggesting a general shift toward higher surface areas per lipid at higher temperatures, and at PSM at 55 ^{o}C, we find great comparison between the experimental literature and both the all-atom and united-atom simulations from this research.

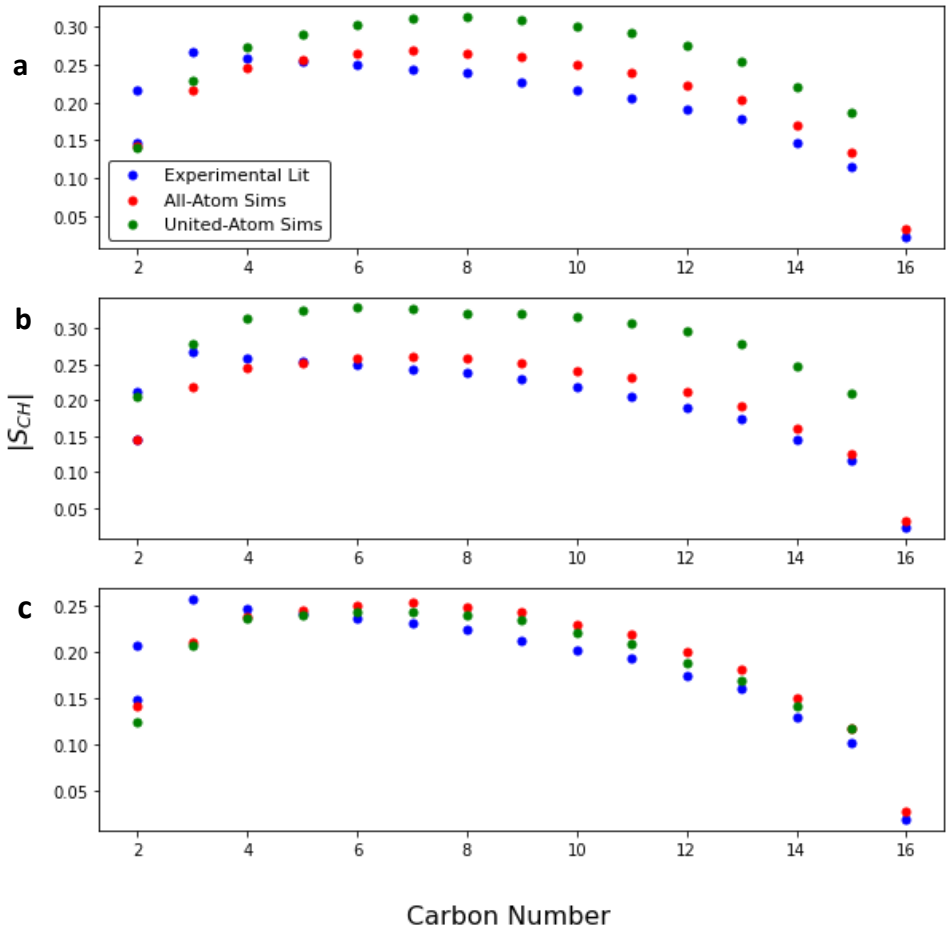

Figure 2.7: Deuterium order parameters for the fatty acid chains for PSM at select temperatures (a – 45 ^{o}C, b – 48 ^{o}C, c – 55 ^{o}C)

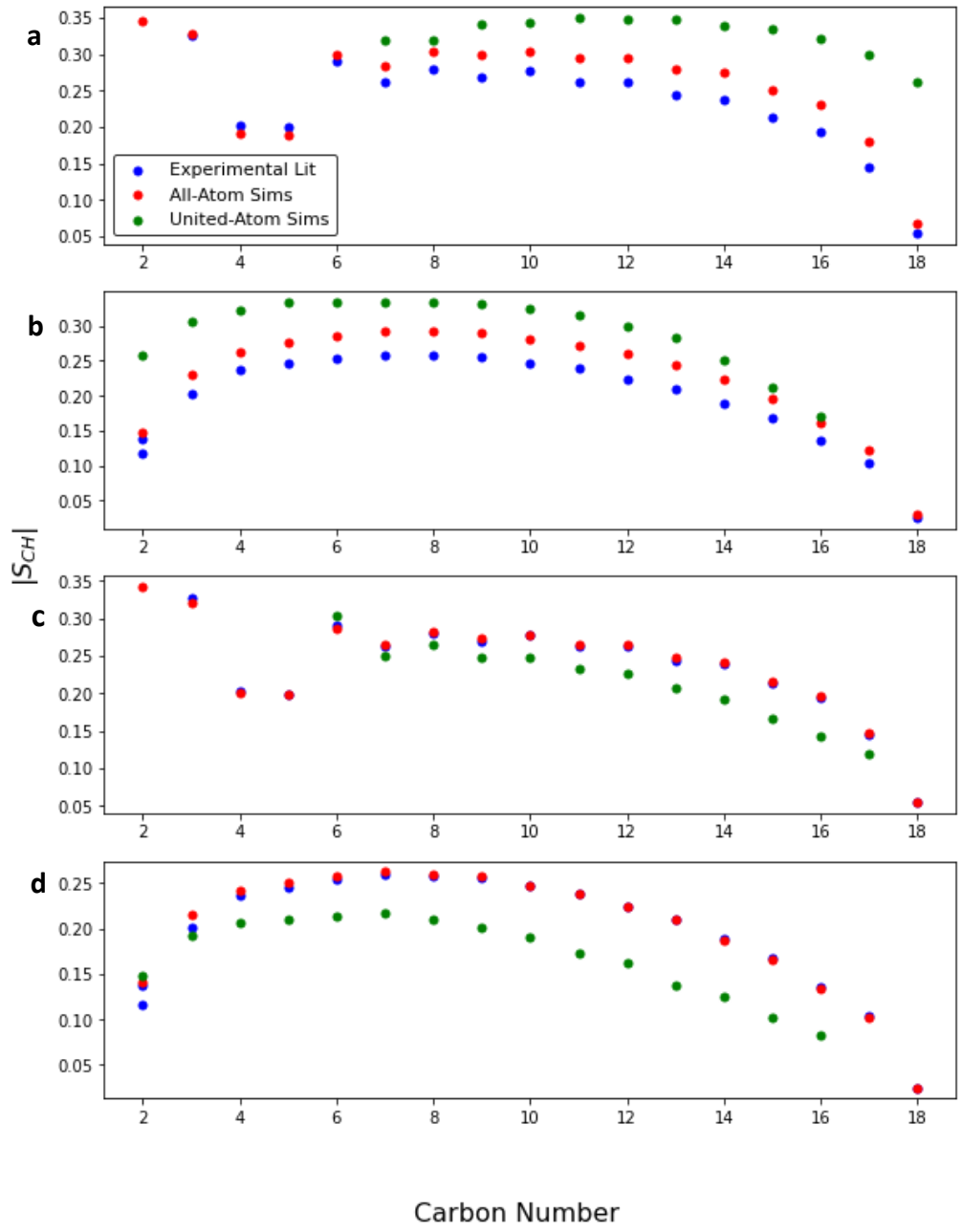

Figure 2.8: Deuterium order parameters for the sphingosine (a, c) and fatty acid (b, d) chains for SSM at select temperatures (a and b - 45 ºC, c and d - 50 ºC)

2.3.3 Electron Density Profiles and Subsequent Properties

Below are presented the Electron Density Profiles for comparison. Electron Density Profiles are provided PSM at 45 ^{o}C and 55^{o}C over the average of three trials to show the reader how the EDPs for the united-atom representations at this point in the research compared to those of the previously defined all-atom representations at temperatures below and above 50 ^{o}C. The experimental and computational electron density profile data themselves were not provided. However, many EDP plots are provided in the experimental and computational literature for the reader to view. To supplement for this, the membrane thicknesses for all experimental temperature comparisons, as well as that for the X-ray Scattering Data for PSM at 45^{o}C, that have been provided are included below.

From the Electron Density Profiles, we find great agreement between the all-atom curves (blue dashed curves) and the united-atom curves (red solid lines) for those simulations above 50 ^{o}C. However, for those simulations below 50^{o}C, we do not find goodness of fit as the united atom simulations are in the gel phase. This was seen for all membrane simulations in their respective phases. Electron Density Profiles will differ depending on the particular phase of the membrane, so this is to be expected. However, ideally, both of these temperatures should be in the liquid phase, as the phase transition should occur at around 40 ^{o}C for sphingomyelin. Once the dihedrals of the lipids are fixed, the phase transition should be lowered to a more accurate temperature, and better fits for the EDPs below 50^{o}C should be seen.

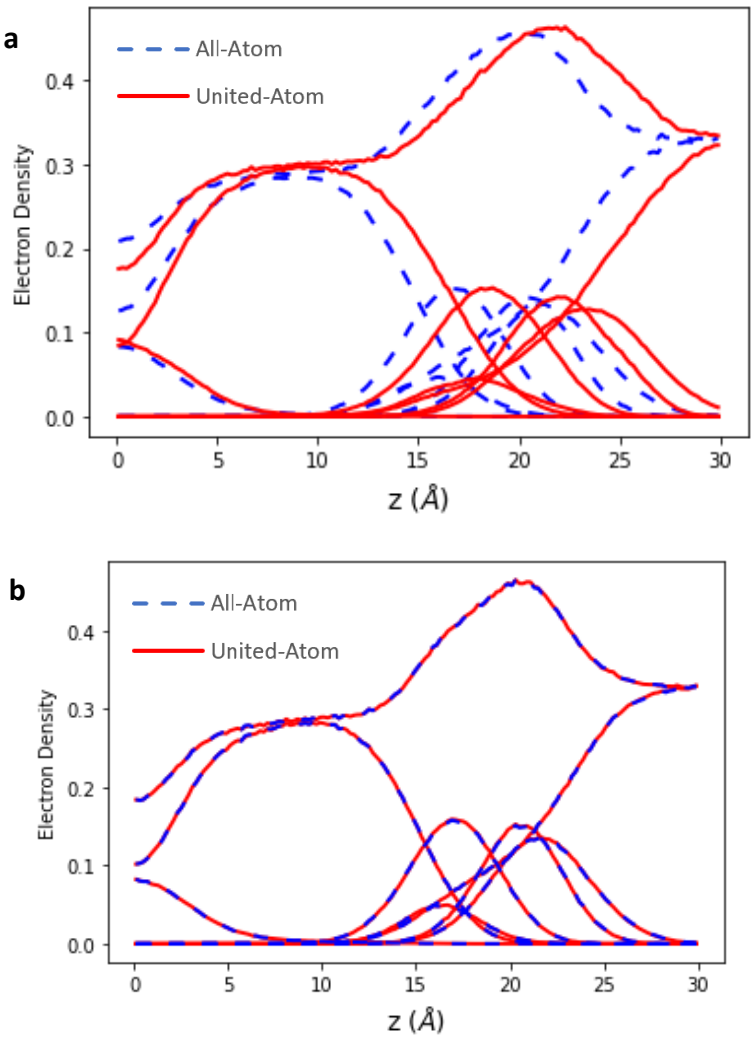

Figure 2.9: Electron Density Profiles for PSM in the gel phase (45 ºC, a) and liquid phase (55 ºC, b). Ideally, PSM should be in the liquid phase at both temperatures.

A table of the membrane thickness comparison is provided in table 2.4. As one can see, the membrane thicknesses for the united-atom and all-atom simulations are slightly higher than those of the experimental literature. This is most likely related to the fact that the all-atom representations for sphingolipids predate the experimental literature by about 10 years. As such, a lipid force field adjustment for the all-atom representations should be warranted. Since the united atom simulations were based on

these simulations, along with the fact that these themselves need their own adjustments as discussed previously, these surface area per lipids are also slightly higher. It should also be noted that the membrane thicknesses for the united-atom simulations are higher for PSM at 45 ºC since these simulations were in the gel state.

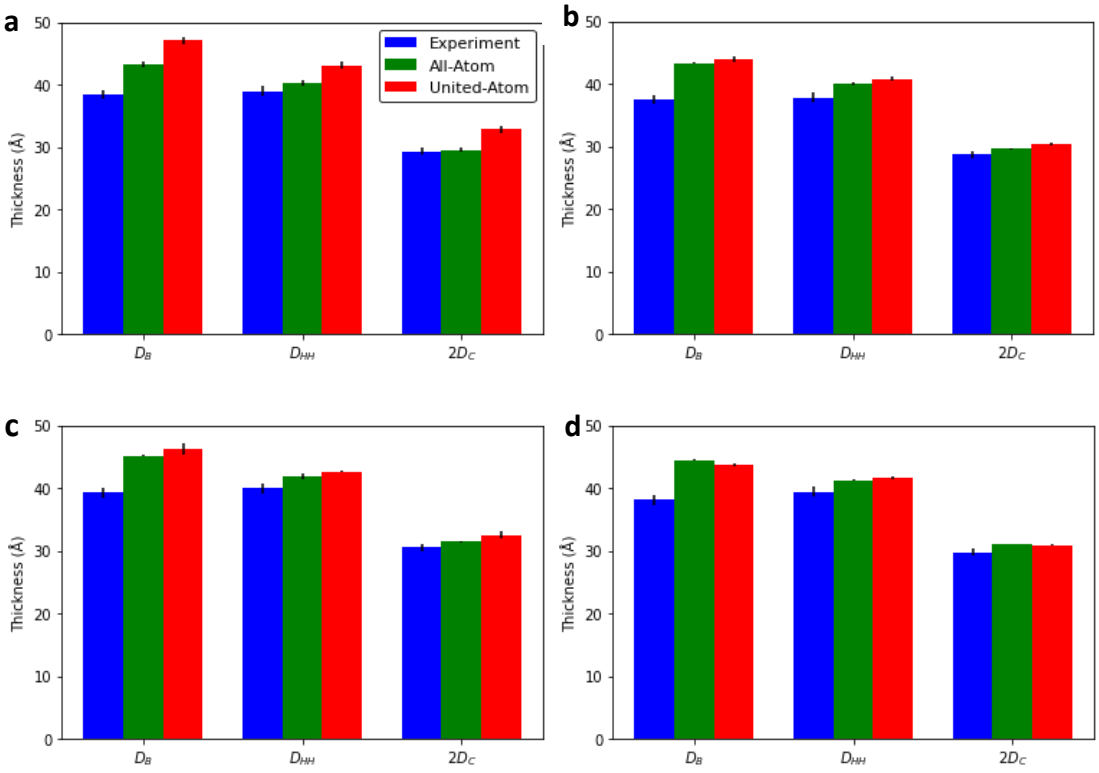

Figure 2.10: Comparison of the membrane thicknesses of the all-atom simulations and united-atom simulations as compared to experimental data[64] for PSM at 45 ºC (a) and 55 ºC (b), and for SSM at 55ºC (c) and 65ºC (d)

The final property that was calculated was the X-ray Scattering Profile form factors. As mentioned, only the PSM at 45ºC was available at the time of writing this thesis. However, once provided, it is expected for us to have all X-ray Scattering data

from Doktorova et. al.[64] to compare with our computational data. Figure 2.9 shows the experimental x-ray data versus our all-atom form factor (top) and united-atom form factor (bottom). As one can see, the all-atom comparison shows nice agreement with experiments. However, the united-atom comparison does not, which is due to the mismatching in the electron density, as shown in figure 2.8 and the phase transition happening at too high a temperature. As such, we reemphasize the need to reexamine the dihedrals of the lipids and phase transition temperature to resolve this issue.

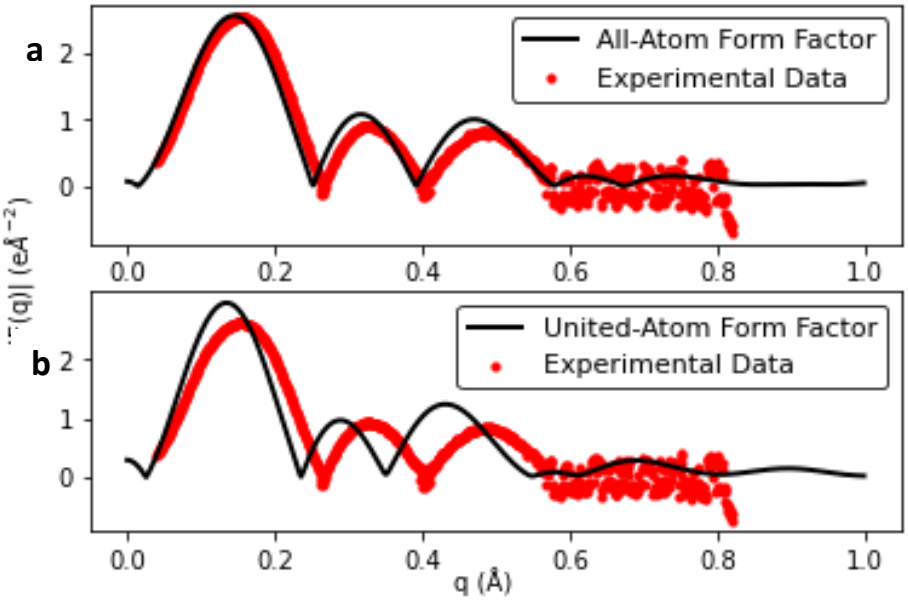

Figure 2.11: Experimental X-ray Scattering Profile (in red) as compared to that of the all-atom (figure a, solid black) and united atom (figure b, solid black) form factors

With the results now calculated and the findings now analyzed, we now move onto the final portion of this thesis. The last chapter will summarize these results and provide future direction for this project, as well as the expected outcomes as the result of this project.

Chapter 3: Conclusions, and Future Directions

Discussion and Conclusions

In conclusion, much progress has been made in this project. The dihedral fitting for the model compounds has been finalized, and what is left now is to scale the simulations up for lipid bilayer simulations. Although for now some of the results are askew due to the dihedrals of the lipid simulations not fitting properly resulting in the phase transition being too high, the results for those simulations above the phase transition match closely with previous computation, and for the surface area per lipid, even match more closely to experimental data than those of the all-atom results. As such there is promise that once the dihedrals are fit for the lipid bilayer simulations, the united-atom simulation will be ready to go aside from any minor tweaks.

The main portion that is left with this research is to fix the dihedrals for the lipid simulations. It is apparent that something is happening in the lipid bilayer simulations that is producing this lack of fit in the lipid. Simulations are currently running to see whether this is a result of the lipid itself, or whether something is happening when the lipids are put in the bilayer. Once this problem is resolved, there may be some small tweaks, such as in the Lennard-Jones parameters, if needed to improve the accuracy as compared with experiment. However, with the dihedral fitting over, the limiting step of this project has now been completed, and we should see the research progress more smoothly.

Future Directions

Once the lipid bilayer simulations have been finalized and the accuracy of the simulations established, the united-atom representation should be ready to be implemented into the CHARMM force field. One final aspect of this research that is planned is to simulate this representation with cholesterols. In nature, sphingolipids do not occupy membrane lipids alone, but are joined by other types of lipids, especially cholesterols. Adding cholesterols in with the sphingolipids would help verify the accuracy and usability of our new model. Afterwards, a united-atom representation for cholesterols is planned. Right now, CHARMM includes an all-atom representation for phospholipids, sphingolipids, and cholesterols, but only a united-atom representation for phospholipids[9]. With the addition of sphingolipids and cholesterols, there would be a full, comprehensive united-atom representation for lipids.

Bibliography

1. Brooks, B. R.; Bruccoleri, R. E.; Olafson, B. D.; States, D. J.; Swaminathan, S.; Karplus, M. CHARMM: A program for macromolecular energy, minimization, and dynamics calculations. *Journal of Computational Chemistry* **1983**, *4* (2), 187-217. DOI: 10.1002/jcc.540040211

2. Brooks, B. R.; Brooks, C. L.; MacKerell, A. D.; Nilsson, L.; Petrella, R. J.; Roux, B.; Won, Y.; Archontis, G.; Bartels, C.; Boresch, S.; et. al. CHARMM: The biomolecular simulation program. *Journal of Computational Chemistry* **2009**, *30* (10), 1545-1614. DOI: 10.1002/jcc.21287

3. Huang, J.; Rauscher, S.; Nawrocki, G.; Ran, T.; Feig, M.; de Groot, B. L.; Grubmüller, H.; MacKerell, A. D. CHARMM36m: An Improved Force Field for Folded and Intrinsically Disordered Proteins. *Nature Methods* **2017**, *14* (1), 71-73. DOI: 10.1038/nmeth.4067

4. Pastor, R. W.; Mackerell, A. D. Development of the CHARMM Force Field for Lipids. *Journal of Physical Chemistry Letters* **2011**, *2* (13), 1526-1532. DOI: 10.1021/jz200167q

5. Klauda J. B.; Venable R. M.; MacKerell A. D.; Pastor R. W. Considerations for lipid force field development. *Computational Modeling of Membrane Bilayers* **2008**, *60*, 1–48 DOI: 10.1016/S1063-5823(08)00001-X

6. Klauda J. B.; Venable R. M.; Freites J. A.; O'Connor J. W.; Tobias D. J.; Mondragon-Ramirez C.; Vorobyov I.; MacKerell A. D.; Pastor R. W.; Update of the CHARMM All-Atom Additive Force Field for Lipids: Validation on Six Lipid Types. *Journal of Physical Chemistry B* **2010**, *114* (23), 7830–7843. DOI: 10.1021/jp101759q

7. Hénin, J.; Shinoda, W.; Klein, M. L. United-Atom Acyl Chain for CHARMM Phospholipids. *Journal of Physical Chemistry B* **2008**, *112* (23), 7008-7015 DOI: 10.1021/jp800687p

8. Lee, S.; Tran, A.; Allsopp, M.; Lim, J. B.; Hénin, J.; Klauda, J. B. CHARMM36 United Atom Chain Model for Lipids and Surfactants. *Journal of Physical Chemistry B* **2014**, *118* (2), 547-556. DOI: 10.1021/jp410344g

9. Yu, Y; Klauda, J. B. Update of the CHARMM36 United Atom Chain Model for Hydrocarbons and Phospholipids. *Journal of Physical Chemistry B* **2020**, *124* (31), 6797-6812. DOI: 10.1021/acs.jpcb.0c04795

10. Metropolis, N.; Rosenbluth, A. W.; Rosenbluth, M. N.; Teller, A. H.; Teller, E. Equation of State Calculations by Fast Computing Machines. *Journal of Chemical Physics* **1953**, *21* (6), 1087-1092. DOI: 10.1063/1.1699114

11. Alder, B. J.; Wainright, T. E. Phase Transition for a Hard Sphere System. *Journal of Chemical Physics* **1957**, *27* (5), 1208-1209. DOI: 10.1063/1.1743957

12. Hastings, W.K. Monte Carlo Sampling Methods Using Markov Chains and Their Applications. *Biometrika*. **1970**, *57* (1), 97-109. DOI: 10.1093/biomet/57.1.97

13. Rahman, A. Correlations in the Motion of Atoms in Liquid Argon. Physical Review **1964**, 136, A405. DOI: 10.1103/PhysRev.136.A405

14. Ciccotti, G.; Dellago, C.; Ferrario, M.; Hernández, E. R.; Tuckerman, M. E. Molecular simulations: past, present, and future (a Topical Issue in EPJB). *The European Physical Journal B* 2022, *95*, 3. DOI: 10.1140/epjb/s10051-021-00249-x

15. Ceperley, D. M.; Alder, B. Ground State of the Electron Gas by a Stochastic Method. *Physical Review Letters* **1980**, *45*, 566-569. DOI: 10.1103/PhysRevLett.45.566

16. Ceperley, D. M.; and Alder, B. J. Ground state of solid hydrogen at high pressures. *Physical Review B* **1987**, *36*, 2092-2106. DOI: 10.1103/PhysRevB.36.2092

17. Frenkel, D.; McTague, J. P. Evidence for an Orientationally Ordered Two-Dimensional Fluid Phase from Molecular-Dynamics Calculations. *Physical Review Letters* **1979**, *42*, 1632-1635. DOI: 10.1103/PhysRevLett.42.1632

18. Frenkel, D.; Mulder, B. M.; and McTague, J. P. Phase Diagrams of Hard Ellipsoids. *Physical Review Letters* **1984**, *52*, 287-290. DOI: 10.1103/PhysRevLett.52.287

19. McCammon, J. A.; Gelin, B. R.; Karplus, M. Dynamics of folded proteins. *Nature* **1977**, *267* (5612), 585-590. DOI: 10.1038/267585a0

20. Case, D. A.; Aktulga, H. M.; Belfon, K.; Ben-Shalom, I. Y.; Berryman, J. T.; Brozell, S. R.; Cerutti, D. S.; Cheatham, T. E.; Cisneros, G. A.; Cruzeiro, V. W. D.; et. al. Amber 2022 Reference Manual. **2022**, University of California, San Francisco.

21. Abraham, M. J.; Murtola, T.; Schulz, R.; Páll, S.; Smith, J. C.; Hess, B.; Lindahl, E. GROMACS: High performance molecular simulations through multi-level parallelism from laptops to supercomputers. *SoftwareX* **2015**, *1–2*, 19–25. DOI: 10.1016/j.softx.2015.06.001

22. Jorgensen, W. L.; Maxwell, D. S.; Tirado-Rives, J. Development and Testing of the OPLS All-Atom Force Field on Conformational Energetics and Properties of Organic Liquids. *Journal of the American Chemical Society* **1996**, *118* (45), 11225-11236. DOI: 10.1021/ja9621760

23. MacKerell, A. D.; Bashford, D.; Bellot, M.; Dunbrack, R. L.; Evanseck, J. D.; Field, M. J.; Fischer, S.; Gao, J.; Gao, H.; Ha, S.; et. al. All-Atom Empirical Potential for Molecular Modeling and Dynamics Studies of Proteins. *Journal of Physical Chemistry B* **1998**, *102* (18), 3586-3616. DOI: 10.1021/jp973084f

24. Vanommeslaeghe, K.; MacKerell, A. D. CHARMM additive and polarizable force fields for biophysics and computer-aided drug design. *Biochimica et Biophysica Acta* **2015**, *1850* (5), 861-871. DOI: 10.1016/j.bbagen.2014.08.004

25. Venable, R. M.; Sodt, A. J.; Rogaski, B.; Rui, H.; Hatcher, E.; MacKerell, A. D.; Pastor, R. W.; Klauda, J. B. CHARMM All-Atom Additive Force Field for Sphingomyelin: Elucidation of Hydrogen Bonding and of Positive Curvature. *Biophysical Journal* **2014**, *107* (1), 134-145. DOI: 10.1016/j.bpj.2014.05.034

26. Reiher, W. H. Theoretical studies of hydrogen bonding (Thesis). **1985**, Harvard University.

27. MacKerell, A. D.; Banavali, N.; Foloppe, N. Development and current status of the CHARMM force field for nucleic acids. *Biopolymers* **2000**, *56* (4), 257–265. DOI: 10.1002/1097-0282(2000)56:4<257::AID-BIP10029>3.0.CO;2-W.

28. Jo, S.; Kim, T.; Iyer, V. G.; and Im, W. CHARMM-GUI: A Web-based Graphical User Interface for CHARMM. *Journal of Computational Chemistry* **2008**, *29* (11), 1859-1865. DOI: 10.1002/jcc.20945

29. Lee, J.; Cheng, X.; Swails, J. M.; Yeom, M. S.; Eastman, P. K.; Lemkul, J. A.; Wei, S.; Buckner, J.; Jeong, J. C.; Qi, Y.; et. al. CHARMM-GUI Input Generator for NAMD, GROMACS, AMBER, OpenMM, and CHARMM/OpenMM Simulations using the CHARMM36 Additive Force Field. *Journal of Chemical Theory and Computation* **2016**, 12 (1), 405-413. DOI: 10.1021/acs.jctc.5b00935

30. Wu, E. L.; Cheng, X.; Jo, S.; Rui, H.; Song, K. C.; Dávila-Contreras, E. M.; Qi, Y.; Lee, J.; Monje-Galvan, V.; Venable R. M.; Klauda, J. B.; Im, W. CHARMM-GUI Membrane Builder Toward Realistic Biological Membrane Simulations. *Journal of Computational Chemistry* **2014**, *35* (27), 1997-2004 DOI: 10.1002/jcc.23702

31. Jo, S.; Lim, J. B.; Klauda, J. B.; Im, W. CHARMM-GUI Membrane Builder for Mixed Bilayers and Its Application to Yeast Membranes. *Biophysical Journal* **2009**, *97* (1), 50-58 DOI: 10.1016/j.bpj.2009.04.013

32. Jo, S.; Kim, T.; Im, W. Automated Builder and Database of Protein/Membrane Complexes for Molecular Dynamics Simulations. PLoS ONE 2007, 2 (9), e880 DOI: 10.1371/journal.pone.0000880

33. Lee, J.; Patel, D. S.; Ståhle, J. Park, S-J.; Kern, N. R.; Kim, S.; Lee, J.; Cheng, X.; Valvano, M. A.; Holst, O.; et. al. CHARMM-GUI Membrane Builder for Complex Biological Membrane Simulations with Glycolipids and Lipoglycans. *Journal of Chemical Theory and Computation* **2019**, *15* (1), 775-786. DOI: 10.1021/acs.jctc.8b01066

34. Vanommeslaeghe, K.; Hatcher, E.; Acharya, C.; Kundu, S.; Zhong, S.; Shim, J.; Darian, E.; Guvench, O.; Lopes, P.; Vorobyov, I.; Mackerell, A. D. CHARMM general force field: A force field for drug-like molecules compatible with the CHARMM all-atom additive biological force fields. *Journal of Computational Chemistry* **2009**, *31* (4), 671–690. DOI: 10.1002/jcc.21367.

35. Lim, J. B.; Rogaski, B.; Klauda, J. B. Update of the Cholesterol Force Field Parameters in CHARMM. *Journal of Physical Chemistry B* **2012**, *116* (1), 203-210. DOI: 10.1021/jp207925m

36. Leal, A. F.; Suarez, D. A.; Echeverri-Peña, O. Y.; Albarracín, S. L.; Alméciga-Díaz, C. J.; Espejo-Mojica, Á. J. Sphingolipids and their role in health and disease in the central nervous system. *Advances in Biological Regulation* **2022**, *85*, 100900. DOI: 10.1016/j.jbior.2022.100900

37. Fabri, J. H. T. M.; de Sá, N. P.; Malavazi, I.; Del Poeta, M. The dynamics and role of sphingolipids in eukaryotic organisms upon thermal adaptation. *Progress in Lipid Research* **2020**, *80*, 101063. DOI: 10.1016/j.plipres.2020.101063

38. Van Meer, G.; Holthuis, J. C. Sphingolipid transport in eukaryotic cells. *Biochimica et Biophysica Acta* **2000**, *1486* (1), 145-170. DOI: 10.1016/s1388-1981(00)00054-8

39. Breslow, D. K.; Weissman, J. S. Membranes in Balance: Mechanisms of Sphingolipid Homeostasis. *Molecular Cell*, **2010**, *40* (2), 267-279. DOI: 10.1016/j.molcel.2010.10.005

40. Thudichum J.L.W. A Treatise on the Chemical Constitution of the Brain: Based Throughout upon Original Researches. *Glasgow Medical Journal* **1884**, *22*, 363–364.

41. Slotte, J. P.; Ramstedt, B. The functional role of sphingomyelin in cell membranes. *European Journal of Lipid Science and Technology* **2007**, *109* (10), 977-981. 10.1002/ejlt.200700024

42. Kraft, M. Sphingolipid Organization in the Plasma Membrane and the Mechanisms That Influence It. *Frontiers in Cell and Developmental Biology* **2016**, *4*, 154. DOI: 10.3389/fcell.2016.00154

43. Giussani, P.; Prinetti, A.; Tringali, C. The role of Sphingolipids in myelination and myelin stability and their involvement in childhood and adult demyelinating disorders. *Journal of Neurochemistry* **2020**, *156* (4), 403-414. DOI: 10.1111/jnc.15133

44. Olsen, A. S. B.; Færgeman, N. J. Sphingolipids: membrane microdomains in brain development, function and neurological diseases. *Open Biology* **2017**, *7* (5), 170069. DOI: 10.1098/rsob.170069

45. van Echten-Deckert, G.; Herget, T. Sphingolipid metabolism in neural cells. *Biochimica et Biophysica Acta* **2006**, *1758* (12), 1978-1994. DOI: 10.1016/j.bbamem.2006.06.009

46. Schneider, N.; Hauser, J.; Olivera, M.; Cazaubon, E.; Mottaz, S. C.; O'Neill, B. V.; Steiner, P.; Deoni, S. C. L. Sphingomyelin in Brain and Cognitive Development Preliminary Data. *eNeuro* **2019**, *6* (4), ENEURO.0421-18.2019. DOI: /10.1523/ENEURO.0421-18.2019

47. Chakraborty, M.; Jiang, X-C. Sphingomyelin and its role in cellular signaling. *Advances in Experimental Medicine and Biology* **2013**, *991*, 1-14. DOI: 10.1007/978-94-007-6331-9_1

48. Green, D. R. Apoptosis and Sphingomyelin Hydrolysis. *Journal of Cell Biology* **2000**, *150* (1), 5-8. DOI: 10.1083/jcb.150.1.f5

49. Li, G.; Kim, J.; Huang, Z.; St. Clair, J. R.; Brown, D. A.; London, E. Efficient replacement of plasma membrane outer leaflet phospholipids and sphingolipids in cells with exogenous lipids. *Proceedings of the National Academy of*

Sciences of the United States of America **2016**, *113* (49), 14025-14030. DOI: 10.1073/pnas.1610705113

50. Spiegel, S.; Merrill, A. H. Sphingolipid metabolism and cell growth regulation. *FASEB Journal* **1996**, *10* (12), 1388-1397. DOI: 10.1096/fasebj.10.12.8903509

51. Taniguchi, M.; Okazaki, T. The role of sphingomyelin and sphingomyelin synthases in cell death, proliferation and migration-from cell and animal models to human disorders. *Biochimica et Biophysica Acta* **2014**, *1841* (5), 692-703. DOI: 10.1016/j.bbalip.2013.12.003

52. Nikolova-Karakashian, M. N.; Rozenova, K. A. Ceramide in stress response. *Advances in Experimental Medicine and Biology* **2010**, *688*, 86-108. DOI: 10.1007/978-1-4419-6741-1_6

53. Huby, E.; Napier, J. A.; Bailieul, F.; Michaelson, L. V.; Dhondt-Cordelier, S. Sphingolipids: towards an integrated view of metabolism during the plant stress response. *New Phytologist* **2020**, *225* (2), 659-670. DOI: 10.1111/nph.15997

54. Trayssac, M.; Hannun, Y. A.; Obeid, L. M. Role of sphingolipids in senescence: implication in aging and age-related diseases. *Journal of Clinical Investigation* **2018**, *128* (7), 2702-2712. DOI: 10.1172/JCI97949

55. Couttas, T. A.; Kain, N.; Tran, C.; Chatterton, Z.; Kwok, J. B.; Don, A. S. Age-Dependent Changes to Sphingolipid Balance in the Human Hippocampus are Gender-Specific and May Sensitize to Neurodegeneration. *Journal of Alzheimer's Disease* **2018**, *63* (2), 503-514. DOI: 10.3233/JAD-171054

56. Souza, P. C. T.; Alessandri, R.; Barnoud, J.; Thallmair, S.; Faustino, I.; Grünewald, F.; Patmanidis, I.; Abdizadeh, H.; Bruininks, B. M. H.; Wassenaar, T. A. Martini 3: a general purpose force field for coarse-grained molecular dynamics. *Nature Methods* **2021**, *18*, 382-388. DOI: 10.1038/s41592-021-01098-3

57. Leonard, A. N.; Wang, E.; Monje-Galvan, V.; Klauda, J. B. Developing and Testing of Lipid Force Fields with Applications to Modeling Cellular Membranes. *Chemical Reviews* **2019**, *119* (9), 6227-6269. DOI: 10.1021/acs.chemrev.8b00384

58. Schmid, N.; Eichenberger, A. P.; Choutko, A.; Riniker, S.; Winger, M.; Mark, A. E.; van Gunsteren, W. F. Definition and testing of the GROMOS force-field versions 54A7 and 54B7. *European Biophysics Journal* **2011**, *40*, 843-856. DOI: 10.1007/s00249-011-0700-9

59. Kulig, W.; Pasenkiewicz-Gierula, M.; Róg, T. Topologies, structures and parameter files for lipid simulations in GROMACS with the OPLS-aa force field: DPPC, POPC, DOPC, PEPC, and cholesterol. *Data in Brief* **2015**, *5*, 333-336. DOI: 10.1016/j.dib.2015.09.013

60. van Gunsteren W. F.; Billeter S. R.; Eising R. A.; Hünenberger P. H.; Krüger P.; Mark A. E.; Scott W. R. P.; Tironi I. G. Biomolecular Simulation: The GROMOS96 Manual and User Guide. **1996**, Hochschulverlag an der ETH Zürich/Biomos, Zürich/Groningen, The Netherlands

61. Chiu, S. W.; Vasudevan, S.; Jakobsson, E.; Mashl, R. J.; Scott, H. L. Structure of Sphingomyelin Bilayers: A Simulation Study. *Biophysical Journal* **2003**, *85* (6), 3624-3635. DOI: 10.1016/S0006-3495(03)74780-8

62. Guvench, O.; Mackerell, A. D. Automated conformational energy fitting for force-field development. *Journal of Molecular Modeling* **2008**, *14* (8), 667-679. DOI: 10.1007/s00894-008-0305-0

63. Yu, Y.; Krämer, A.; Veneable, R. M.; Simmonett, A. C.; Mackerell, A. D.; Klauda, J. B.; Pastor, R. W.; Brooks, B. R. Semi-automated Optimization of the CHARMM36 Lipid Force Field to Include Explicit Treatment of Long-Range Dispersion. *Journal of Chemical Theory and Computation* **2021**, *17* (3), 1562-1580. DOI: 10.1021/acs.jctc.0c01326

64. Doktorova, M.; Kučerka, N.; Kinnun, J. J.; Pan, J.; Marquardt, D.; Scott, H. L.; Veneable, R. M.; Pastor, R. W.; Wassall, S. R.; Katsaras, J.; Heberle, F. A. Molecular Structure of Sphingomyelin in Fluid Phase Bilayers Determined by the Joint Analysis of Small-Angle Neutron and X-ray Scattering Data. *Journal of Physical Chemistry B* **2020**, *124* (25), 5186-5200. DOI: 10.1021/acs.jpcb.0c03389

65. Durell, S. R.; Brooks, B. R.; Ben-Naim, A. Solvent-Induced Forces between Two Hydrophilic Groups. *Journal of Physical Chemistry A* **1994**, *98*, 2198– 2202. DOI: 10.1021/j100059a038

66. Jorgensen, W. L.; Chandrasekhar, J.; Madura, J. D.; Impey, R. W.; Klein, M. L. Comparison of Simple Potential Functions for Simulating Liquid Water. *Journal of Chemical Physics* **1983**, *79*, 926– 935. DOI: 10.1063/1.445869

67. Phillips, J. C.; Zheng, G.; Kumar, S.; Kale, L. V. In NAMD: Biomolecular Simulation on Thousands of Processors, Proceedings of the 2002 ACM/IEEE Conference on Supercomputing; *IEEE Computer Society Press*, **2002**; pp 1– 18.

68. Wennberg, C. L.; Murtola, T.; Páll, S.; Abraham, M. J.; Hess, B.; Lindahl, E. Direct-Space Corrections Enable Fast and Accurate Lorentz-Berthelot Combination Rule Lennard-Jones Lattice Summation. *Journal of Chemical Theory and Computation* **2015**, *11*, 5737– 5746. DOI: 10.1021/acs.jctc.5b00726

69. Hoover, W. G. Canonical Dynamics: Equilibrium Phase-Space Distributions. *Physical Review A* **1985**, *31*, 1695– 1697. DOI: 10.1103/PhysRevA.31.1695

70. Feller, S. E.; Zhang, Y.; Pastor, R. W.; Brooks, B. R. Constant Pressure Molecular Dynamics Simulation: The Langevin Piston Method. *Journal of Chemical Physics* **1995**, *103*, 4613– 4621. DOI: 10.1063/1.470648

71. Martyna, G. J.; Tobias, D. J.; Klein, M. L. Constant Pressure Molecular Dynamics Algorithms. *Journal of Chemical Physics* **1994**, *101*, 4177– 4189. DOI: 10.1063/1.467468

72. Kučerka, N.; Katsaras, J.; Nagle, J. F. Comparing Membrane Simulations to Scattering Experiments: Introducing the SIMtoEXP Software. *Journal of Membrane Biology* **2010**, *235*, 43– 50. DOI: 10.1007/s00232-010-9254-5